2,4,6-Trimethylbenzoyldiphenylphosphine oxide (TPO) analog: a non-cytotoxic type-I photoinitiator for free radical photopolymerization

Jiansong Yin, Yijun Zhang, Bernadette Graff, Céline Dietlin, Michael Schmitt, Fabrice Morlet-Savary, Tatiana Petithory, Laurent Pieuchot, Jing Zhang, Yangyang Xu, et al.

Novel TPO Analog: A Non-Cytotoxic Type-I Photoinitiator for Free Radical Photopolymerization

Jiansong Yin[a,b,c], Yijun Zhang[b,c], Bernadette Graff[b,c], Céline Dietlin[b,c], Michael Schmitt[b,c], Fabrice Morlet-Savary[b,c], Tatiana Petithory[b,c], Laurent Pieuchot[b,c], Jing Zhang[d], Yangyang Xu[a]*, Jean-Michel Becht[b,c*], Jacques Lalevée[b,c*] and Pu Xiao[e]*

[a]College of Chemistry and Materials Science, Anhui Normal University, South Jiuhua Road 189, Wuhu 241002, P. R. China.

[b]Université de Haute-Alsace, CNRS, IS2M UMR 7361, F-68100 Mulhouse, France.

[c]Université de Strasbourg, France.

[d]Future Industries Institute, University of South Australia Mawson Lakes, SA 5095, Australia

[e]State Key Laboratory of High Performance Ceramics and Superfine Microstructure, Shanghai Institute of Ceramics, Chinese Academy of Sciences, Shanghai 200050, P. R. China

Keywords: Photoinitiator, Photopolymerization, 3D printing, Cytotoxicity

Abstract: 2,4,6-trimethylbenzoyldiphenylphosphine oxide (TPO) is a highly efficient and widely used photoinitiator, but it is currently facing significant concerns regarding cytotoxicity. This work investigates a novel photoinitiator designed as an alternative to TPO. The newly synthesized TPO analog, 6-(2,4,6-trimethylbenzoyl)-(6H)-dibenz[c,e][1,2]oxaphosphorin 6-oxide (TDOPO), incorporating 9,10-dihydro-9-oxa-10-phosphaphenanthrene 10-oxide (DOPO) motif, presents promising characteristics as a Type I photoinitiator. It can be synthesized efficiently in just two steps using commercially available chemicals, without the need for extensive purification procedures. Notably, the TDOPO exhibits absorption close to the visible spectrum, suggesting its potential for use in visible light curing applications. Comparative studies reveal that TDOPO exhibits strong photoinitiation ability for the free radical photopolymerization of acrylate in both thin and thick samples. The photochemical mechanism studies indicate its capability to generate three distinct types of free radicals: 2,4,6-trimethylbenzoyl, oxygen-centered, and phosphorus-centered free radicals. In addition, TDOPO shows no cytotoxicity in a 20-hour assay, a result far superior to that of TPO. These findings underscore the

potential of TDOPO as an effective and safer alternative to TPO in photopolymerization processes.

Introduction

In recent years, the application of near-UV and visible light in the field of photopolymerization has witnessed a notable surge. Light-emitting diodes (LEDs), serving as the primary light source, offer distinct advantages over traditional mercury lamps, including superior safety, environmental compatibility, energy efficiency, cost-effectiveness, stability, and durability. Consequently, there is a pressing demand for novel near-UV and visible light photoinitiators to meet the evolving requirements of photopolymerization. These photoinitiators play a pivotal role in enabling more efficient and precise photopolymerization reactions under LED irradiation [1-7].

Among these, acyldiphenylphosphine oxides, such as commercially available 2,4,6-trimethylbenzoyldiphenylphosphine oxide (TPO), ethyl (2,4,6-trimethylbenzoyl) phenylphosphinate (TPO-L), phenylbis(2,4,6-trimethylbenzoyl) phosphine oxide (BAPO), lithium phenyl-2,4,6-trimethylbenzoylphosphinate (LAP) etc..., have attracted considerable attention because of their exceptional photoinitiation properties within specific wavelength ranges [1,8]. Widely studied for their role in photochemical reactions, these compounds [8-11] are integral to the field of photopolymerization and hold promise for applications in other light-driven chemical processes [12-16].

Moreover, the absorption spectra of acyldiphenylphosphine oxides spans notably from 350 nm to 400 nm [17-21], facilitating the efficient generation of phosphinoyl and acyl radicals through cleavage of carbon-phosphorus bonds, thus allowing the initiation of the photopolymerization process [11,12]. As a typical representative of acylphosphine oxides, 2,4,6-trimethylbenzoyldiphenylphosphine oxide (TPO, Figure 1) has been widely used [20]. However, concerns over its cellular toxicity highlight the imperative to design less toxic TDOPO capable of maintaining photoactivity, thereby advancing safety standards in photochemistry [22]. The active pursuit of novel and highly efficient phosphine oxides is currently a vibrant research area [21]. For instance, a TDOPO was obtained by substituting the 2,4,6-trimethylphenyl group from TPO with a 2,4,6-trimethoxyphenyl group [11]. It led to a 90% conversion in free radical polymerization of cyclic trimethylolpropane formal acrylate (CTFA) at a concentration of 0.1wt% and showed reduced cytotoxicity than TPO [13]. In addition,

various 2,6-dimethyl-4-alkoxyphenyl groups [16] were also used to replace the 2,4,6-trimethylphenyl group in TPO. And the series of molecules synthesized demonstrated good solubility in monomers and exhibited favorable photopolymerization properties. However, the series of compounds synthesized have notable drawbacks, such as low conversions of TMPTA monomers at low light intensity of visible light. In addition, the synthesis process requires an extra purification step. Of particular concern is the fact that synthetic acylphosphine oxide photoinitiators are often unstable and decompose easily at room temperature or even when stored at low temperatures [1, 13, 19].

To address these challenges, we implemented a strategy combining theoretical calculations with experimental approaches. Our method involved initial molecular design aimed at enhancing stability, followed by rigorous theoretical assessments to verify stability under operational conditions. Additionally, we carefully considered the cost implications throughout the synthesis process to optimize efficiency and efficacy.

In this study, we successfully designed and synthesized a new Type I photoinitiator, *i.e.* a 9,10-dihydro-9-oxa-10-phosphaphenanthrene 10-oxide (DOPO)-based phosphine-oxide as an alternative to TPO. This compound has a unique cyclic conjugated structure and is commercially accessible at a low price. In addition, its larger aromatic ring conjugation relative to TPO induces a red-shift in light absorption, broadening excitation range for photopolymerization reactions. Moreover, DOPO is a new generation of environmentally friendly and green new flame retardant modified monomer widely used in the field of flame retardants [23-25]. Therefore, photoinitiators designed based on DOPO are likely to be environmentally friendly and exhibit low cytotoxicity as well. Using real-time Fourier transform infrared (RT-FTIR) spectroscopy, we compared the free radical photopolymerization process of TMPTA under 405 nm LED irradiation between TPO and its DOPO-based analog. Our findings reveal comparable polymerization efficiencies. We further explored the photoinitiation mechanism of the TDOPO through UV-visible photolysis and electron spin resonance (ESR)-spin trapping experiments. Direct laser write (DLW) experiments were conducted to evaluate the potential of TDOPO for substitution in practical applications. The results showed that the TDOPO shares comparable properties with traditional TPO in photopolymerization reactions and exhibits similar photosensitivity ranges. Moreover, the performance of TDOPO in toxicity tests was equally impressive. In a 20-hour cytotoxicity test, TDOPO did not demonstrate

cytotoxicity. Specifically, the number of cells in the cell-culture dish showed a substantial increase, and there was no visible decrease in cell activity. In contrast, the control TPO did not promote cell proliferate and quickly became inactivated. These findings strongly endorsed its potential to replace TPO in practical applications.

2. Experimental Section

2.1. Theoretical computations and molecular modeling

Calculations rely on Density Functional Theory (DFT) using the Gaussian software. Ground state and triplet state geometries have been optimized for the TDOPO studied in this paper and for TPO used as a comparison at the UB3LYP/6-31G(d) level of theory. The same is true for the radicals used for the bond dissociation energy (BDE) calculations and for the spin density computation. The lowest unoccupied molecular orbital (LUMO) and the highest occupied molecular orbital (HOMO) listed in Table 1 and Table S1 have been computed in a single point at a RTD-mPW1PW91-FC/6-31G* level of theory on the previously optimized geometries.

2.2. General remarks

2,4,6-Trimethylbenzaldehyde (mesal), 9,10-dihydro-9-oxa-10-phosphaphenanthrene 10-oxide (DOPO), 2,4,6-trimethylbenzoyldiphenylphosphine oxide (TPO), Dess-martin periodinane (DMP), trimethylolpropane triacrylate (TMPTA), dichloromethane (DCM), ethyl acetate (AcOEt), phenyl-N-*tert*-butylnitrone (PBN), *tert*-butylbenzene were purchased from Sigma-Aldrich and were used directly without additional purifications (See Figure 1). ^{1}H-NMR, ^{13}C-NMR, and ^{31}P-NMR spectra were performed at ambient temperature using a Varian Oxford 300 MHz spectrometer and $CDCl_3$ as the solvent, with the chemical shifts in ^{1}H-NMR aligned to the solvent peak of $CHCl_3$ in the deuterated solvent (7.26 ppm). A Bruker high-resolution mass spectrometer (HRMS) was used to record high-resolution mass spectra.

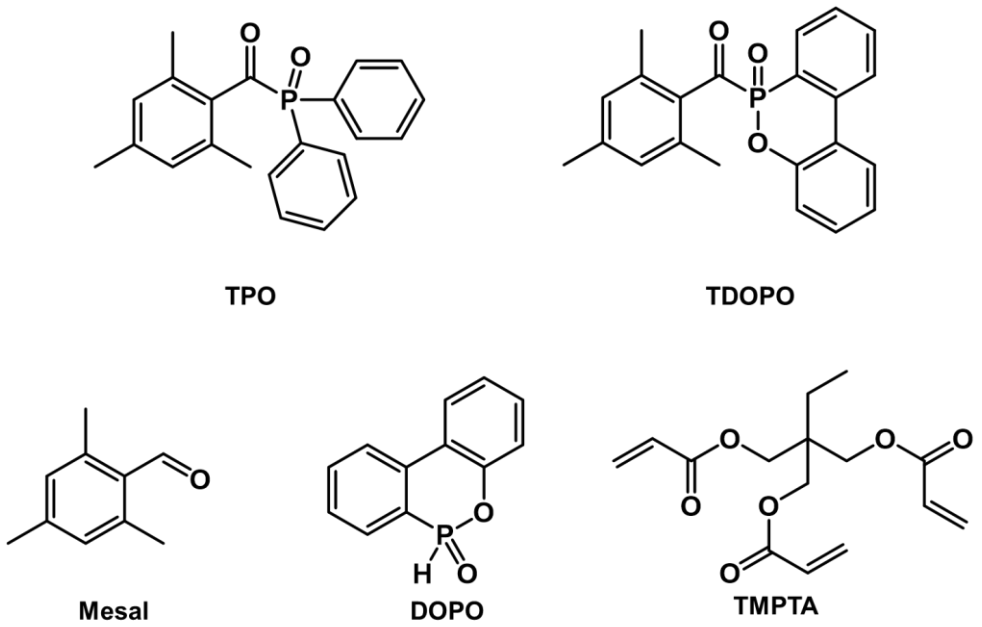

Figure 1. Key chemical compounds synthesized and/or used in this work.

2.3. Synthesis of the TDOPO

Step 1: Synthesis of (10-Oxo-10H-9-oxa-10λ^5-phospha-phenanthren-10-yl)-(2,4,6-trimethylphenyl)methanol (Alc-1): mesal (3.0 equiv., 6 mmol, 889 mg) and DOPO (1.0 equiv., 2 mmol, 432 mg) were introduced successively into a dry flask. The reaction mixture was then stirred at room temperature for 24 hours. After reaction, the reaction mixture was filtered through a sand core funnel to afford a white solid. This solid was then washed with AcOEt (3×25 mL) and dried under vacuum (0.1 mbar). Alc-1 was obtained with > 95% purity and was therefore directly used in the second step without additional purifications (white powder, 656 mg, 90% isolated yield, mixture of two diastereoisomers). ^{1}H NMR (300 MHz, $CDCl_3$) δ (ppm): 8.07 - 7.67 (m, 4H), 7.50 - 7.15 (m, 4H), 6.63 and 6.69 (s, 2H), 5.77 - 5.65 (m, 1H), 2.21 (s, 3H), 2.18 (s, 6H). ^{31}P NMR (121 MHz, $CDCl_3$) δ (ppm): 32.7, 32.1. ^{13}C NMR (75 MHz, $CDCl_3$) δ(ppm): 149.7, 137.6 (d, *J* = 3 Hz), 133.7 (d, *J* = 2.3 Hz), 132.0 (d, *J* = 9 Hz), 131.5, 130.4, 130.3, 128.5 (d, *J* = 12.8 Hz), 128.2 (d, *J* = 12 Hz), 127.6, 124.7, 124.5, 124.2, 124.1, 123.2 (d, *J* = 9 Hz), 121.7, 121.4, 119.9, 119.8, 71.1 (d, *J* = 107 Hz), 30.9, 20.7, 20.6. (Detail in supporting information Figure S1, S2, S3). HRMS (ESI): m/z calculated for $[C_{22}H_{21}NaO_3P]^+$: 387.1121, found: 387.1119.

Step 2: TDOPO: Dess-Martin periodinane (1.5 equiv., 3 mmol, 1.27 g) was added to a solution of Alc-1 (1 equiv., 2 mmol, 728 mg) in DCM (2 mL). The reaction mixture

was then vigorously stirred in the dark for 4 h and quenched with an aqueous saturated solution of Na_2SO_3 (3 mL). The resulting mixture was then extracted with AcOEt (20 mL). The organic phase was washed successively with aqueous saturated solutions of $NaHCO_3$ (15 mL) and Na_2SO_3 (15 mL). The organic phase was then concentrated under vacuum. A yellow gel with a purity > 95% was obtained and no additional purifications were required (661mg, 91% isolated yield). ^{1}H NMR (300 MHz, $CDCl_3$) δ(ppm): 8.05 - 7.84 (m, 3H), 7.77 (m, 1H), 7.54 (m, 1H), 7.28-7.15 (m, 2H), 7.07 (d, *J* = 8.1 Hz, 1H), 6.81 (s, 2H), 2.24 (s, 3H), 2.09 (s, 6H). ^{31}P NMR (121 MHz, $CDCl_3$) δ(ppm): 10.5. ^{13}C NMR (75 MHz, $CDCl_3$) δ(ppm): 213.7 (d, *J* = 110 Hz), 149.3, 149.2, 140.5, 137.2 (d, *J* = 6.8 Hz), 136.0, 135.4, 134.7, 134.5 (d, *J* = 2.2 Hz), 132.0 (d, *J* = 10.5 Hz), 130.8, 128.8, 128.6, 125.0 (d, *J* = 6.8 Hz), 123.8 (d, *J* = 9.8 Hz), 122.0, 121.6, 121.5 (d, *J* = 10.5 Hz), 120.1 (d, *J* = 6.8 Hz), 21.2, 19.4. (Detail in supporting information Figure S4, S5, S6). HRMS (ESI): m/z calculated for $[C_{22}H_{19}NaO_3P]^+$: 385.0964, found: 385.0961.

2.4. UV-visible spectroscopy experiments

The ultraviolet-visible spectra were performed using a Jasco V-730 spectrometer in a quartz cell with DCM as the solvent. In experiments involving steady-state photolysis, a photoinitiator solution in DCM underwent irradiation using LED@385 nm (100 mW/cm^2), followed by capturing UV-vis spectra at varying time of irradiation. The concentrations of the TDOPO and TPO stood at 0.2 mM, with the spectral data presented in Figure 2 and Figure 3.

2.5. Quantum yield of photolysis

The quantum yield (Φ) of photolysis was gauged using constant irradiation in a DCM solution. The quantum yield of photolysis for TPO was quantified according to the value reported in reference [33] (The value of Φ_{TPO} was 0.56). The subsequent formula computes the quantum yield of photolysis for the novel photoinitiator:

$$\Phi_{sample} = \Phi_{TPO}[\varepsilon_{TPO} \cdot slope_{sample}]/[\varepsilon_{sample} \cdot slope_{TPO}]$$

where the slope represents the slope of the function $\ln[\exp(2.3OD_{385\ nm\ at\ different\ irradiation\ time}) - 1] = f(t)$ (OD: the optical density or absorption)[11, 14].

2.6. The electron spin resonance spin-trapping (ESR-ST) experiment

ESR-ST experiments were carried out using an X-band spectrometer (Bruker

EMX-plus) to investigate the free radicals produced upon irradiation. Samples were prepared by using *tert*-butylbenzene as a solvent and purging with nitrogen at room temperature for 3 min. Free radicals generated by LED 385 nm (100 mW/cm^2) irradiation of TDOPO (0.5 mM) and TPO (0.5 mM) are captured and detected. Phenyl-N-*tert*-butylnitrone (PBN) was used as a spin-trap agent. The radical adducts generated by the addition of the primary radicals onto PBN can be observed and characterized.

2.7. RT-FTIR spectroscopic analysis

To obtain photocurable samples, 2.80×10^{-5}mol g^{-1} photoinitiator was added straightly to the trifunctional acrylate monomer trimethylolpropane triacrylate (TMPTA) and stirred overnight until it was dissolved. To track the C=C double bond conversion over time during the photopolymerization of a sample measuring 2 mm or 25μm in thickness, a Jasco 6600 real-time Fourier transform infrared spectrometer (RT-FTIR) was employed. Each photopolymerization test was conducted in air at ambient temperature. The decrease of the acrylate C=C double bond peak is monitored at approximately 1630 cm^{-1} for thin films and approximately 6150 cm^{-1} for thick films, respectively. In the photopolymerization tests, a 405 nm LED emitting 100 mW/cm^2 of light was employed to cure the photosensitive resins. To calculate the double bond conversions over time (DC_t), the following formula was used [26]:

$$DC_t = [(A_0 - A_t)/ A_0]\times100\%$$

where A_0 represents the acrylate functional group's peak area at 0 seconds, and A_t denotes the acrylate functional group's peak area at t seconds.

2.8. 3D printing experiments with direct laser writing (DLW)

3D printing experiments were carried out using a modified laser engraving machine (NEJE-DK3000). The 1.40×10^{-5}mol g^{-1} PIs in TMPTA formulations are used. Then, DLW were carried out using a homemade glass container that was about 2 mm thick to hold the formulations, and a laser diode at 405 nm was used for the spatially controlled irradiation.

2.9. Scanning electron microscope (SEM) experiments

The SEM (JEOL JSM-7900F) was used to examine the printed 3D patterns. The images were obtained at an accelerating voltage of 2 kV.

2.10. Cytotoxicity experiments

For cell morphology, proliferation and time-lapse imaging, a Holomonitor® M4 phase holographic microscope (PHI AB, Lund, Sweden) was used with a 10 times phase contrast objective, placed in an incubator at 37°C and 5% CO_2. The C3H10 T1/2 cells lines were seeded in a 6 well plate (Sarstedt AG & Co. KG, Germany) the day before the test to attach at 20000 cells/well in Dulbecco's modified eagle medium (DMEM) 10 vol% fetal bovine serum (FBS). The concentration used for each PI is 50µM. The medium with this concentration of PI was replace just before to start the acquisition. The lid of the 6-well plate was replaced with the HoloLid® 71120 for 6-well plate (PHI AB) and then placed on the motorized stage of the HoloMonitor® M4 in the incubator. Images were acquired at 10 locations per well, at 30 minutes' intervals for 20 hours.

3. Results and discussion

3.1. Molecular modeling of the **TDOPO**

Initially, molecular modeling was performed to assess the characteristics of the TDOPO, focusing on specific criteria. Firstly, the compound should exhibit a good light absorption in the near UV and UV ranges, particularly around 360-400 nm. Therefore, it was necessary to compute the oscillator strength (related to the absorption) and maximum absorption wavelength (λ_{max}) mainly corresponding to the HOMO-LUMO transition (Table 1). Secondly, efficient cleavage of the α bond of the 2,4,6-trimethylbenzoyl group was essential for optimal performance as a type I photoinitiator. This required favorable C(O)-P covalent bond cleavage under irradiation and the bond cleavage enthalpy from the excited triple state ($\Delta H = BDE\text{-}E_T$) needed to be negative or close to 0 kcal/mol (detailed in supporting information Table S1). It is important to note that there was about 3-4 kcal/mol of uncertainty in the DFT calculations at the UB3LYP/6–31G(d) level of theory [11, 13, 27]. Therefore, the cleavage reaction can still be beneficial for compounds with slightly positive ΔH values. For the TDOPO, ΔH was calculated as -2.1 kcal/mol, whereas it was 0.2 kcal/mol for TPO. This indicated that, this cleavage reaction was favorable for the TDOPO from the triplet excited state after light absorption. Furthermore, evaluation of spin densities on the radical centers ($P^{\bullet}$ and $C^{\bullet}$) was crucial, as higher localization of spins can suggest greater reactivity but also less stabilized free radicals. For the

TDOPO, the spin densities around $P^{\bullet}$ and $C^{\bullet}$ were 0.492 and 0.646, respectively, compared to 0.481 and 0.646 for TPO (detail in supporting Information Figure S7, S8). Based on the molecular modelling results, the TDOPO can exhibit: i) good near-UV absorption properties, ii) efficient cleavage ability of the C(O)-P bond, and iii) generation of potentially reactive i.e. less stabilized radicals. Based on these findings, it was decided to proceed with synthesizing the TDOPO in the next phase of the study.

Table 1. Highest occupied molecular orbitals (HOMO) and Lowest unoccupied molecular orbital (LUMO) were calculated for the TDOPO and TPO

Photoinitiator	Molecular structure	HOMO	LUMO
TPO	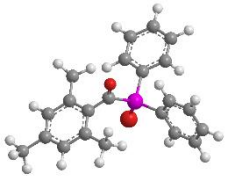	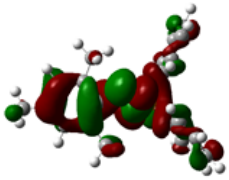	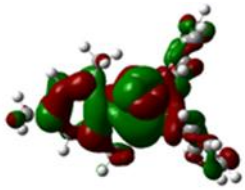
TDOPO	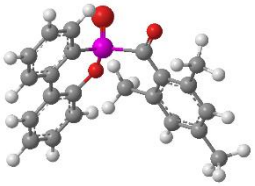	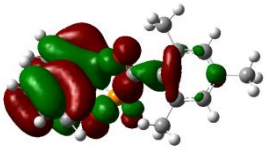	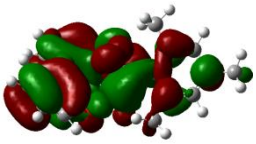

3.2. Synthesis of the TDOPO

Molecular modelling indicated promising potential for TDOPO as a type I photoinitiator, prompting its synthesis from commercially available 2,4,6-trimethylbenzaldehyde (mesal) and DOPO. The synthesis was performed in two steps: 1) nucleophilic addition of DOPO to mesal to form an alcohol; 2) oxidation of the alcohol to yield the desired TDOPO. In the first step, both compounds were initially reacted in ethyl acetate using a recently described experimental procedure [12,15]. However, this resulted in complicated reaction mixtures and a low yield of the desired alcohol. Subsequent addition of triethylamine and sodium carbonate as bases did not improve the yields. Referring to previous literature, DOPO was then reacted with mesal under neat conditions for 24 hours at room temperature [28, 29], affording the expected alcohol in a high yield (90%). For the oxidation step,

commercially available activated MnO_2 was initially used, but a complex reaction mixture was obtained. Subsequently, activated MnO_2 was replaced by the Dess-Martin periodinane and the TDOPO was generated with a yield of almost 91% [30, 31]. Notably, both Alc-1 and the TDOPO were produced in pure form directly after synthesis, eliminating the need for further purification steps. Scheme 1 outlines the final chemical route used for the synthesis of the TDOPO.

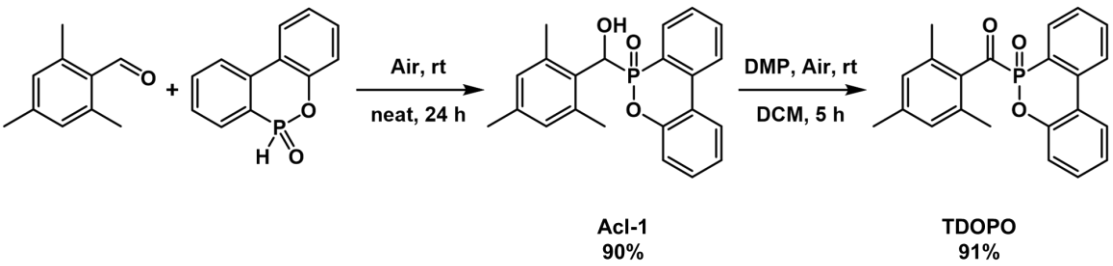

Scheme 1. Synthetic route of TDOPO

3.3 Stability tests of the TDOPO

The storage stability of photoinitiators significantly influences their practical applications. To assess this, we conducted stability tests on the TDOPO. For this purpose, the TDOPO was stored in an airtight, air-filled container at room temperature, shielded from light exposure. ^{1}H-NMR analysis was performed after 3 months, and no obvious degradation was observed when compared with the ^{1}H-NMR spectrum of the freshly synthesized TDOPO (see Figure S4 and S9 in the supporting information). This indicates that the storage conditions effectively preserved the molecular integrity of the TDOPO over the testing period.

3.4 The spectroscopic properties of the TDOPO

The UV-visible absorption spectra of TPO and its analog were captured in DCM. Figure 2 illustrates their absorption bands near 380 nm, closely aligning with the emission spectra of near UV LED (e.g. 385, 395, or 405 nm). The maximum absorption wavelength of TDOPO showed a slight redshift of around 5 nm compared to TPO, although its extinction coefficient was lower. This low extinction coefficient for TDOPO vs. TPO suggested a more significant n-π^* character in its absorption band [32]. There was a good agreement between the computed (Table S1) and observed (Figure 2) spectra, with the computed wavelength maxima (Table S1) closely matching the experimental ones in DCM (380 nm for TPO and 385 for the

TDOPO).

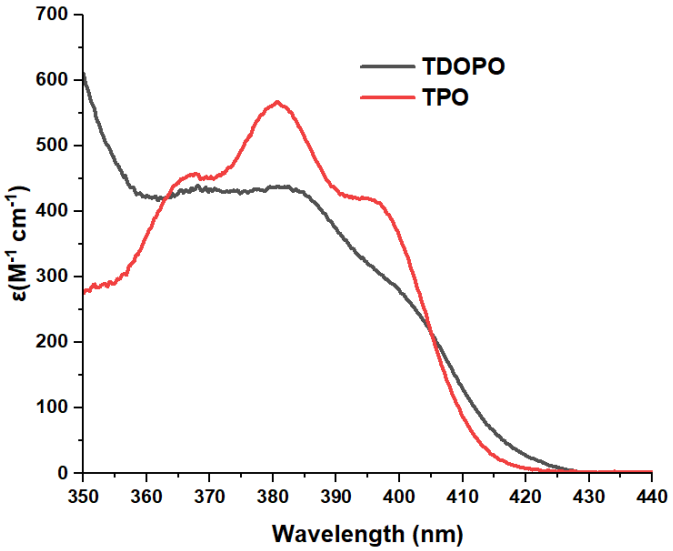

Figure 2. UV-visible absorption spectra of TPO and TDOPO in the range from 350 nm to 440 nm (in DCM solvent).

The electronic transition details and frontier molecular orbitals shown in Table 1 help elucidate the changes in the light absorption of TDOPO. For acylphosphine oxide photoinitiators, the lowest energy transition occurs in the n-π* transition. Analysis of the electron cloud distribution of TDOPO reveals that during its transition from LUMO to HOMO, some electrons from the electron cloud located on the DOPO group transfer to the 2,4,6-trimethylbenzoyl group, which causes a slight red shift in its UV-visible spectrum. This phenomenon underscores the significant role of the DOPO group in the HOMO and LUMO.

3.5. Photochemical properties and cleavage ability

Using a UV-visible spectrophotometer, steady-state photolysis studies were carried out in DCM to investigate the photochemical behavior of TPO and TDOPO. Figure 3 illustrates that the UV-visible absorption of the PIs solution under a LED@385 nm irradiation steadily droped as the irradiation time increased within the wavelength range of 350-420 nm. No new absorption peak was observed, indicating that the photoproducts generated by the cleavage of the P-C bond of the PIs did not exhibit absorption in the 350-440 nm wavelength range throughout the photodegradation process. To further elucidate the cleavage reaction, the photolysis quantum yield of the TDOPO was estimated.

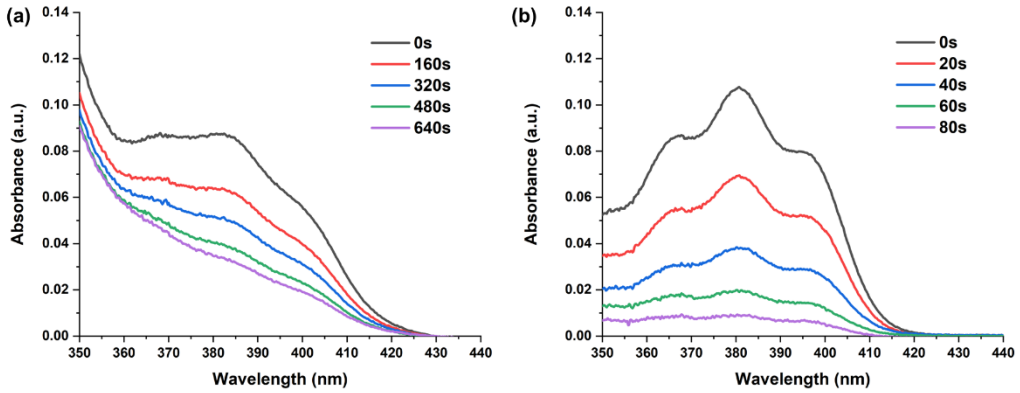

Figure 3. UV-vis absorption spectra recorded during steady-state photolysis of the TDOPO and TPO (0.2 mM in DCM) under LED@385 nm (100 mW/cm²) irradiation. (a) TDOPO and (b) TPO.

To study the cleavage reaction, we investigated the quantity of molecules undergoing α cleavage as a function of photon absorption. The experimental analysis (Figure 4) elucidates that the TDOPO quantum yield Φ is 0.061 (Φ_{TPO} = 0.56, as reported in ref. [33]). Despite its lower Φ value, our thorough examination of the TDOPO's UV-visible absorption and its promising theoretical calculations prompted further characterization efforts.

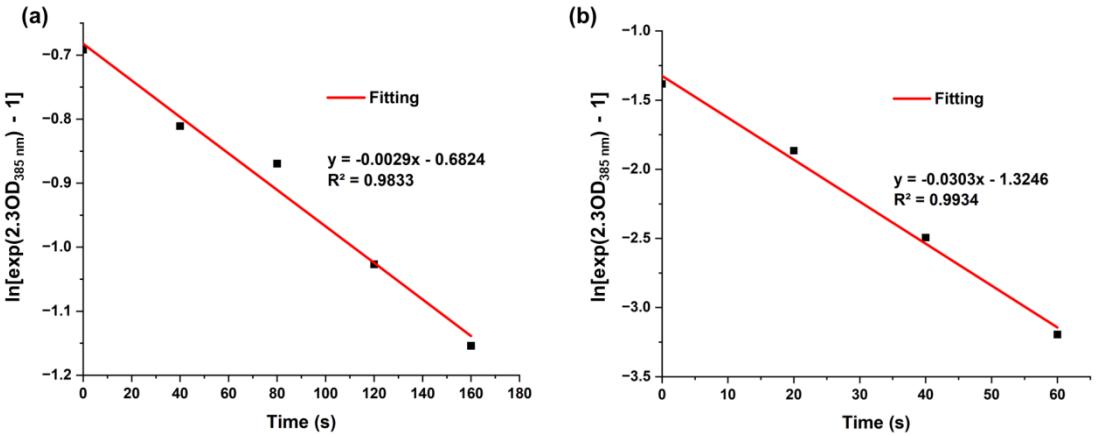

Figure 4. The slope of the function: (a) TDOPO, and (b) TPO.

The potentially reactive radicals produced via C-P bond cleavage of the TDOPO under a 385 nm LED irradiation were then studied by ESR-ST experiments (Figure 5) [33]. For the PBN spin adducts, the simulation yields distinctive hyperfine coupling constants [12, 34, 35]: one free radical species (48.7%) exhibits the following characteristics: a_N = 14.1 G; a_H = 3.3 G; a_P = 20.1 G and a_H = 1.4 G, with a second

radical species (51.3%) showing a_N=13.0 G and a_H=1.3 G. The first radical species belongs to that centered on phosphorus (Scheme 2), whereas the second one might belong to the oxygen-centered radical [34] as shown in Scheme 2. However, 2,4,6-trimethylbenzoyl radical cannot be detected when using PBN as a spin-trap [34]. Theoretical computer simulations, prompted by unexpected experimental outcomes, verified the feasibility of oxygen-centered radical formation. This was supported by spin density calculation surrounding oxygen, computed at 0.259 (details in supporting information Figure S8).

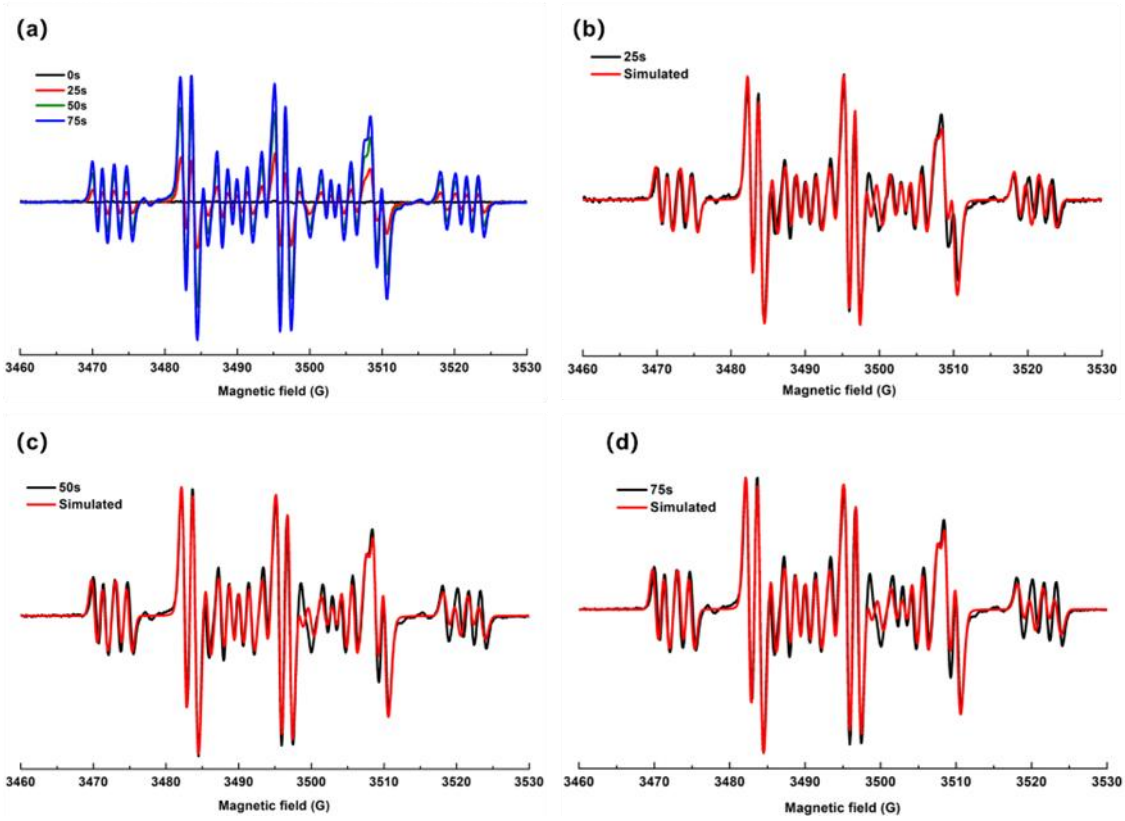

Figure 5. The PBN radical adducts (ESR-ST spectra using *tert*-butylbenzene as a solvent) for TDOPO. (a) the spectrum detected at 0s, 25s, 50s, and 75s; (b) (c) (d) The simulations at 25s, 50s, and 75s (LED@405 nm irradiation).

Consequently, these experimental and theoretical insights suggest plausible chemical pathways as summarized in Scheme 2. Upon light exposure, the TDOPO transitions from its ground state to an excited state. Two different types of radicals can be produced through the homolytic cleavage of C-P bonds in TDOPO. The phosphinoyl radical may equilibrate with an oxygen-centered radical during these processes. This mechanism also differs from conventional acylphosphine oxide photoinitiators [16].

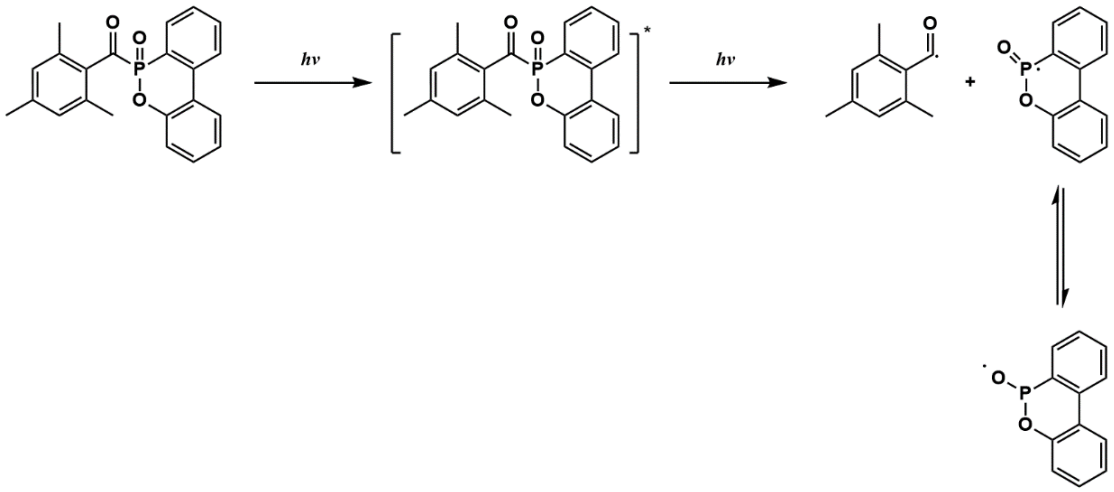

Scheme 2. Proposed photofragmentation mechanism of TDOPO.

3.6. Free radical polymerization experiments of TMPTA

The commercially available TPO was selected as a reference due to its high solubility and good initiation efficiency with acrylate photocuring systems. In this study, we compared the photopolymerization performance of the TDOPO in TMPTA under an LED@405 nm irradiation (Figure 6a). The comparison indicates that the TDOPO achieves a photoinitiation efficiency comparable to that of TPO when exposed to 405 nm light (photoinitiator concentration 2.80×10^{-5}mol g^{-1} in TMPTA), suggesting its potential as a substitute under similar conditions. Furthermore, we investigated the photoinitiation capacity of the TDOPO at various concentrations in TMPTA (0.28×10^{-5} mol g^{-1} ~ 2.80×10^{5} mol g^{-1}). As shown in Figures 6c and 6d, the polymerization reactions were efficient across all investigated PI concentrations. This suggested the superior photoinitiation efficiency of the phosphinoyl radicals produced from the TDOPO compared to those generated from TPO (as the light absorption and the cleavage efficiency were lower for the new proposed PI vs. TPO as previously discussed). Thin film (thickness: 25μm) experiments (Figure 6b), further underscored the good polymerization rate and polymerization conversion of TDOPO vs. to commercial TPO. Based on these findings, the TDOPO was used to perform 3D printing experiments using a DLW set-up. The 3D patterns (letters "CNRS", “CRM”, “HY”) were successfully printed (Figure 7a). Subsequent SEM characterization of the printed letter “R” (Figure 7b) confirmed its structural integrity and fidelity.

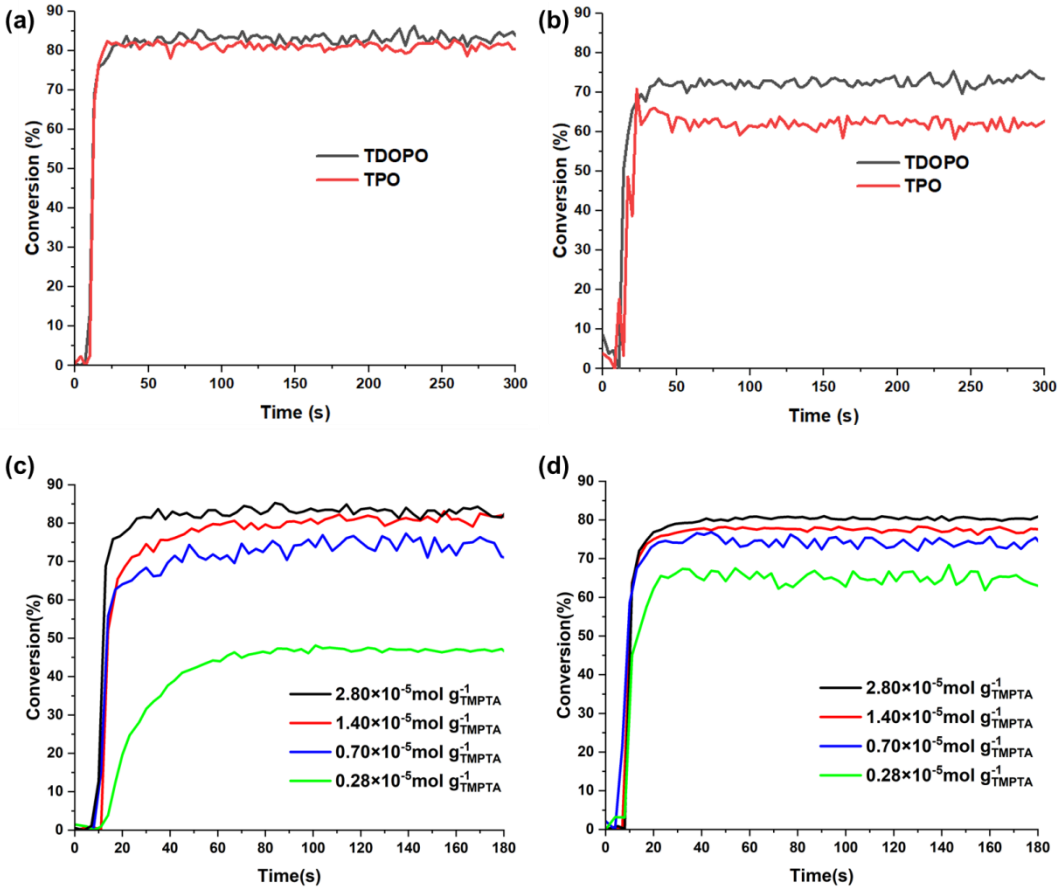

Figure 6. Photopolymerization profiles of TMPTA thick sample (acrylate functions conversion vs. time) thickness = 2 mm, under air, using LED@405nm (100 mW/cm^2), irradiation starts at t = 10 s. (a) 2.80×10^{-5}mol g$^{-1}_{TMPTA}$ TDOPO compared with 2.80×10^{-5}mol g$^{-1}_{TMPTA}$ TPO; (b) Polymerization curves of TMPTA films in the concentration of 2.80×10^{-5}mol g$^{-1}_{TMPTA}$ PIs (thin sample, thickness=25µm, under air, using LED@405 nm, irradiation starts at t = 10 s). (c) 0.28×10^{-5}mol g$^{-1}_{TMPTA}$ ~ 2.80×10^{-5}mol g$^{-1}_{TMPTA}$ TDOPO under irradiation at 405 nm (thick sample, irradiation starts at t = 10 s); (d) 0.28×10^{-5}mol g$^{-1}_{TMPTA}$ ~ 2.80×10^{-5}mol g$^{-1}_{TMPTA}$ TPO under irradiation at 405 nm (thick sample; irradiation starts at t = 10 s).

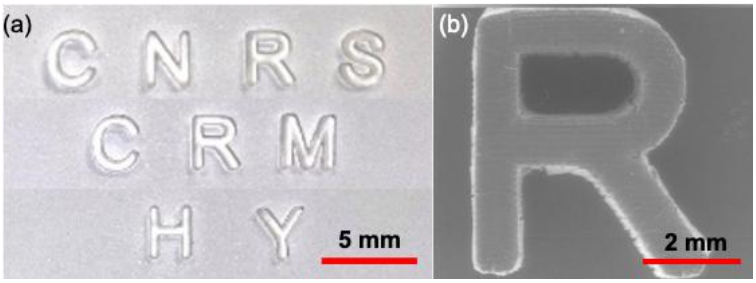

Figure 7. (a) Direct laser writing of the 3D patterns (thickness = 1mm). (b) SEM characterization of the letter R printed by DLW, top view of the letter R.

3.7. Evaluation of photoinitiator cytotoxicity

It is well known that TPO has long been difficult to use on a large scale for long-term future applications due to its cytotoxicity [22]. Therefore, there is an urgent need for a non-cytotoxic photoinitiator that can enble a wide range of future applications. Here we investigate whether the modifications made to the TPO molecule to produce TDOPO result in reduced cytotoxicity. We compare the effect of TPO and TDOPO on the proliferation and migration kinetics of murine C3H10 T1/2 mesenchymal cells. We use the HoloMonitor® M4 label-free live imaging system to track cell movement and division over 18h in the presence of the two components (Figure 8 and supporting information Figures S10, S11 and S12). We use the concentration of 50 µM that is known to induce toxicity. We found that TPO had a dramatic effect on cell proliferation and migration. Cells stopped moving and dividing a few minutes after treatment (Figure 8e, 8g, 8h, and supporting information video S1 and S2). Cell shape analysis shows that most cells adopted a round shape (Figure 8a, 8b, 8i), with some cells detaching from the surface, further indicating the induction of cell death within the population. On the other hand, the cell population treated with TDOPO increases gradually over time. Cell tracking further show that cells are migrating at normal speed for this cell type (Figure 8f, 8g, 8h, and supporting information video S3 and S4). This suggests that cells treated with TDOPO proliferated and migrated normally, highlighting the lack of toxicity of the new molecule. Shape analysis shows that cells spread correctly on the surface, confirming they are not affected by the molecule. These findings indicate that that the modifications to the structure of the molecule greatly reduce its toxicity without affecting its performance.

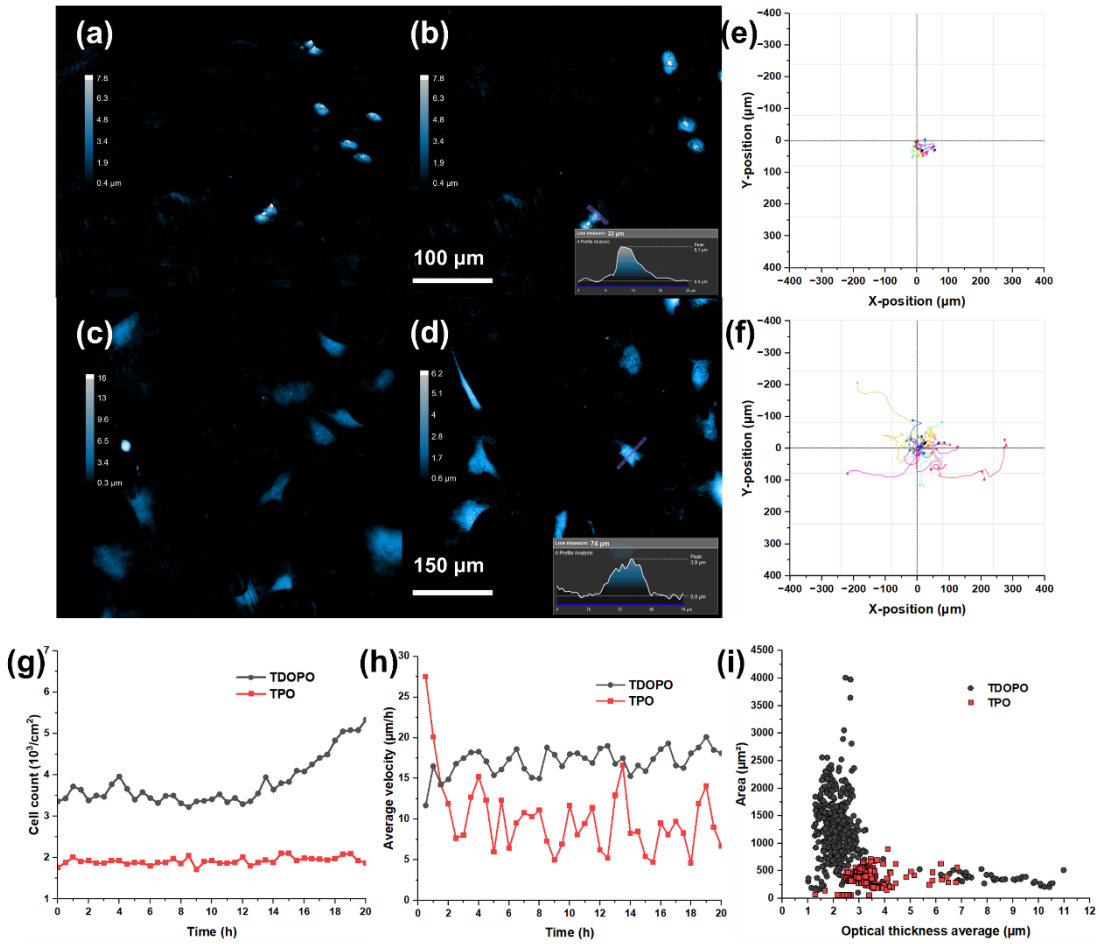

Figure 8. (a) and (b) are TPO treated C3H10 T1/2 cell lines holographic phase images, (c) and (d) C3H10 T1/2 cell lines imaged were TDOPO treatment (Randomly selecting different locations for imaging, the left color band in the figure represents C3H10 T1/2 cell lines thickness, the small graph in the lower right corner of both Figures b and c is a profile analysis). (e) TPO treatment experimental group single cell tracking image. (f) TDOPO treatment experimental group single cell tracking image. (g) Comparison of cell number counts in TPO treatment experimental group and TDOPO treatment experimental group. (h) Comparison of cells mobility velocity in TPO treatment experimental group and TDOPO treatment experimental group. (i) Cell morphology analysis image.

4. Conclusion

In summary, a new TDOPO photoinitiator was successfully synthesized in this work, which demonstrated excellent solubility in the acrylate monomer used and exhibited outstanding photoinitiation ability. Specifically, it efficiently induced the photopolymerization of TMPTA, achieving high polymerization rates and final conversions. Moreover, the synthesis process was straightforward, utilizing cost-effective raw materials that were readily accessible at a laboratory scale and more economical than those required for TPO (Table S2). In addition, this photoinitiator

proved to be non-cytotoxic. Given these advantages, the TDOPO presents itself as a promising alternative to TPO. Its introduction is anticipated to set new standards in photoinitiator performance, thereby promoting advancements in photopolymerization technology. This innovation can expand the horizon of photoinitiator research and holds significant potential for diverse applications across various sectors. This critical step will contribute to its broader adoption and ensure its suitability for industrial and commercial applications.

Declaration of Competing Interest

The authors declare that they have no known competing financial interests or personal relationships that could have appeared to influence the work reported in this paper.

Acknowledgments

This work was performed under the National Natural Science Foundation of China (Grant No. 22105005) and HPC resources of the Mesocentre of the University of Strasbourg and the HPC resources from GENCI-IDRIS (Grant 2023-AD010812313R2/Jean_Zay). Thanks to Loïc Vidal (CNRS, IS2M, UMR 7361) for helping us complete the SEM tests in this work. We are also grateful to Dr. Didier Le Nouën (CNRS, LIMA, UMR 7042) for NMR analyses, and to Dr. Cécile Joyeux (CNRS, LIMA, UMR 7042) for HRMS analyses.

References

[1] S. M. Müller, S. Schlögl, T. Wiesner, M. Haas, T. Griesser, ChemPhotoChem 2022, 6, 1-13.

[2] M.Mitterbauer, P. Knaack, S. Naumov, M. Markovic, A. Ovsianikov, N. Moszner, R. Liska, Angew. Chem. Int. Ed. 2018, 57, 12146 -12150.

[3] Z. Q. Li, X. C. Zou, F. Shi, R. Liu, Y. Yagci, Nat. Commun. 2019, 10, 3560.

[4] A. Kocaarslan, K. Kaya, S. Jockusch, Y. Yagci, Angew. Chem. Int. Ed. 2022, 61, e202208845

[5] J. Kirschner, F. Szillat, M. Bouzrati-Zerelli, J. M. Becht, J. E. Klee, J. Lalevée, J. Polym. Sci., Part A: Polym. Chem. 2019, 57, 1664.

[6] H. Mokbel, D. Anderson, R. Plenderleith, C. Dietlin, F. Morlet-Savary, F. Dumur, D. Gigmes, J. P. Fouassier, J. Lalevée, Polym. Chem. 2017, 8, 5580.

[7] T. Gao, Y. Zhang, F. Morlet- Savary, B. Graff, J. Zhang, P. Xiao, F. Dumur, J. Lalevée, Small 2024, DOI: 10.1002/smll.202400234.

[8] M. Bouzrati-Zerelli, J. Kirschner, C. P. Fik, M. Maier, C. Dietlin, F. Morlet-Savary, J. P. Fouassier, J. M. Becht, J. E. Klee, J. Lalevee, Macromolecules 2017, 50, 6911.

[9] X. Kuang, J. T. Wu, K. J. Chen, Z. Zhao, Z. Ding, F. J. Y. Hu, D. N. Fang, H. J. Qi, Sci. Adv. 2019, 5, 5790.

[10] J. Zhang, D. Campolo, F. Dumur, P. Xiao, J. P. Fouassier, D. Gigmes, J. Lalevee, ChemCatChem 2016, 8, 2227.

[11] C. Dietlin, T. T. Trinh, S. Schweizer, B. Graff, F. Morlet-Savary, P. A. Noirot, J. Lalevée, Macromolecules 2019, 52, 7886-7893.

[12] Y. P. Wu, R. Li, J. Ke, X. Cheng, R. Tang, Y. Situ, H. Huang, Eur. Polym. J. 2022, 168, 111093.

[13] L. Buchon, J. M. Becht, L. Rubatat, W. Wang, H. Wei, P. Xiao, J. Lalevee, J. Appl. Polym. Sci. 2023, 140, 1-14.

[14] C. Dietlin, T. T. Trinh, S. Schweizer, B. Graff, F. Morlet-Savary, P. A. Noirot, J. Lalevée, Molecules 2020, 25, 1-9.

[15] Y. Liu, T. Wang, C. Xie, X. Tian, L. Song, L. Liu, Z. Wang, Q. Yu, Prog. Org. Coatings 2020, 142, 105603.

[16] Y. Wu, J. Ke, C. Dai, J. Wang, C. Huang, Y. Situ, H. Huang, Eur. Polym. J. 2022, 175, 111380.

[17] H. F. Sobhi, J. M. Masnovi, A. T. Riga, J. Therm. Anal. Calorim. 2010, 101, 1065-1069.

[18] R. Nazir, P. Danilevicius, D. Gray, M. Farsari, D. T. Gryko, 2013, 46, 7239-7244.
[19] D. Zhao, Y. Liu, Q. Wang, Y. Zhang, X. Zhang, Y. Du, T. Wang, Prog. Org. Coatings 2024, 187, 108110.
[20] C. Xie, Z. Wang, Y. Liu, L. Song, L. Liu, Z. Wang, Q. Yu, Prog. Org. Coatings 2019, 135, 34-40.
[21] C. Decker, K. Zahouily, D. Decker, T. Nguyen, T. Viet, Polymer 2001, 42, 7551-7560.
[22] B. Zeng, Z. Cai, J. Lalevée, Q. Yang, H. Lai, P. Xiao, J. Liu, F. Xing, Toxicol. In Vitro, 2021, 72,105103.
[23] H. Wang, Q. Liu, X. Zhao, Z. Jin, Polym. Degrad. Stab. 2021, 183, 109440.
[24] C. D. Varganici, L. Rosu, A. Bifulco, D. Rosu, F. Mustata, S. Gaan, Polym. Degrad. Stab. 2022, 202, 110020.
[25] K. A. Salmeia, S. Gaan, Polym. Degrad. Stab. 2015, 113, 119-134.
[26] X. Y. Zhao, Y. Zhao, M. D. Li, Z. A. Li, H. Y. Peng, T. Xie, X. L. Xie, Nat. Commun. 2021, 12, 2873.
[27] R. Sure, J. G. Brandenburg, S. Grimme, ChemistryOpen 2016, 5, 94-109.
[28] R. Bai, R. Choudhary, P. Singh, R. Thakuria, M. C. Sharma, S. S. Badsara, ChemistrySelect 2018, 3, 3221-3224.
[29] N. K. Gusarova, N. A. Chernysheva, B. A. Trofimov, Synth. 2017, 49, 4783-4807.
[30] B. Zhang, J. He, Y. Li, T. Song, Y. Fang, C. Li, J. Am. Chem. Soc. 2021, 143, 4955.
[31] S. D. Meyer, S. L. Schreiber, J. Org. Chem. 1994, 59, 7549-7552.
[32] S. Sun, S. Liang, W. C. Xu, G. Xu, S. Wu, Polym. Chem. 2019, 10, 4389-4401.
[33] S. Jockusch, I. V. Koptyug, P. F. McGarry, G. W. Sluggett, N. J. Turro, D. M. Watkins, J. Am. Chem. Soc. 1997, 119, 11495-11501.
[34] A. Criqui, J. Lalevée, X. Allonas, J. Fouassier, Macromol. Chem. Phys. 2008, 209, 2223-2231.
[35] L. Breloy, C. Negrell, A.-S. Mora, W. S. Jennifer Li, V. Brezová, S. Caillol, D. L. Versace, Eur. Polym. J. 2020, 132, 109727.

TOC graphic:

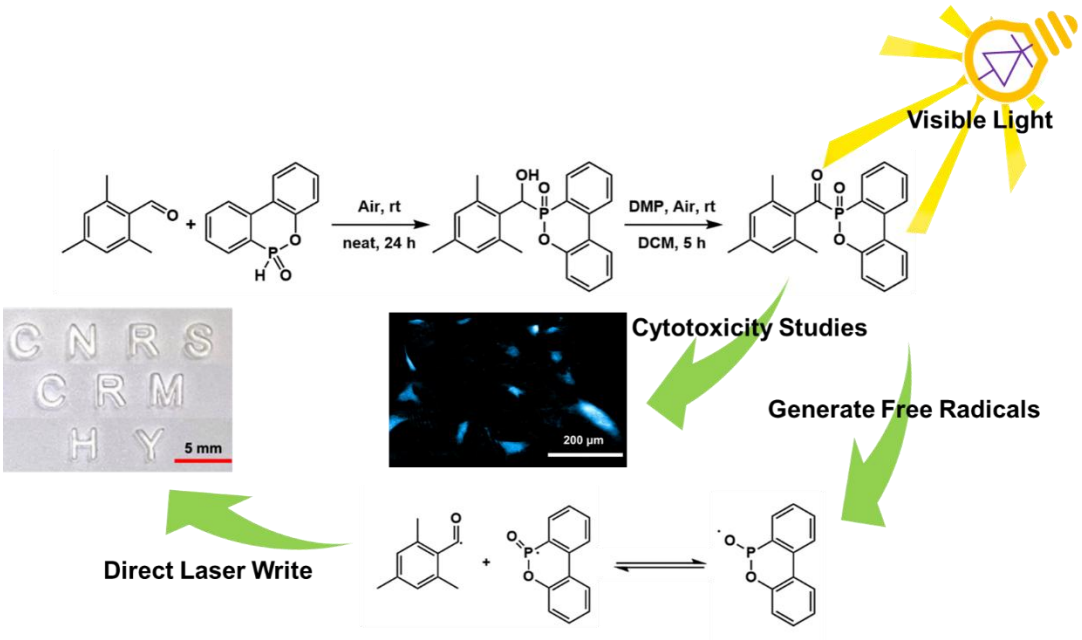
Visible Light
Air, rt
neat, 24 h
DMP, Air, rt
DCM, 5 h
Cytotoxicity Studies
Generate Free Radicals
Direct Laser Write
5 mm
200 µm